



# The Effects of Cycle Frequency on Mechanical Behavior of Rock Salt for Energy Storage

Yue Han<sup>1</sup> · Hongling Ma<sup>2</sup> · Hao Cui<sup>1</sup> · Ning Liu<sup>1</sup>

Received: 21 January 2022 / Accepted: 22 July 2022 / Published online: 2 September 2022  
© The Author(s), under exclusive licence to Springer-Verlag GmbH Austria, part of Springer Nature 2022

## Abstract

Salt caverns are used to store different energy sources, resulting in different periodic operating frequencies. To investigate the influence of the cycle frequencies on the mechanical behavior of rock salt, uniaxial stepped cyclic loading tests with successively decreasing, successively increasing and arbitrarily changing frequency were conducted. The deformation and dissipated energy under different frequencies were compared and analyzed. The test results demonstrate that the cycle frequency slightly affects the deformation evolution and that effect only appears when the adjacent frequencies change sharply (more than 50 times). The strain induced in one frequency stage (stage deformation) caused by high frequency is greater than that at low frequency. The dissipated energy is affected significantly by frequency. The individual dissipated energy decreases nearly as a power function with the frequency, while the stage dissipated energy shows the opposite trends due to the large increase of the loading cycles. In general, a quick injection and withdrawal is more dangerous for surrounding rock. The results are helpful for the operation of salt cavern used for energy storage.

## Highlights

- A novel test method with good accuracy and reliability—‘stepped varying frequencies at the same cyclic stress’ is conducted to study the effect of frequency.
- Deformation of rock salt is slightly affected by the changing frequency.
- The individual dissipated energy decreases with the increase of frequency, while the accumulated dissipated energy in a frequency stage shows the opposite.
- The damage and deformation of the rock surrounding a salt cavern are relatively large when the cyclic loading is fast.

**Keywords** Energy storage · Stepped cyclic loading tests · Cycle frequency · Dissipated energy · Deformation

## 1 Introduction

It is widely agreed that cyclic loading is more damaging than monotonic loading to the stability of rocks surrounding salt storage caverns, because fatigue failure may occur when

the peak amplitude of the cyclic loading is lower than the monotonic strength and even the yield strength. In geotechnical engineering, rock may be subjected to cyclic loading induced by periodic storage and release of water, periodic injection and withdrawal of compressed air, periodic traffic flow, etc. Many researchers have investigated the mechanical characteristics of rocks under cyclic loading, including the basic mechanical performance (Chen et al. 2018, 2016; Guo et al. 2018), the factors that influence fatigue (Peng et al. 2019; Liu et al. 2018; Han et al. 2020), the damage evolution (Zhao et al. 2021; Peng et al. 2020a, b), as well as the constitutive laws of fatigue behavior (Hu et al. 2019; Ma et al. 2017; Khaledi et al. 2016).

Since the influencing factors that affect the mechanical behavior during or following cyclic loading are derived from

✉ Yue Han  
hanpyue@163.com

✉ Hongling Ma  
hlma@whrsm.ac.cn

<sup>1</sup> PowerChina Huadong Engineering Corporation Limited, Hangzhou 310014, Zhejiang, China

<sup>2</sup> State Key Laboratory of Geomechanics and Geotechnical Engineering, Institute of Rock and Soil Mechanics, Chinese Academy of Sciences, Wuhan 430071, Hubei, China

engineering conditions, the exploration of these factors is critical to solving the actual problems. The stress-related factor involves the maximum stress, the minimum stress, the stress amplitude, and the mean stress. The time-related factor includes frequency. Other related factors are the loading waveform and the interval duration (Fan et al. 2020). Based on extensive experimental research, the effects of some factors are clear and are generally accepted. For example, the fatigue life decreases obviously with the increase of the maximum stress. However, the effects of some factors are still ambiguous, such as the cycle frequency.

The cycle frequency is the operating frequency. Underground salt caverns are used widely for energy storage owing to their good tightness and mechanical properties (Yin et al. 2018; Jiang et al. 2016). The operating frequencies vary by different applications. For different applications, the operating frequencies differ. To meet the seasonal demands, the operating frequency for storing natural gas is annual, but for compressed air energy storage, daily injection and withdrawal are applied. The mechanical behaviors under different frequencies are vitally important for designing the operating scheme for different applications.

To assess the influence of cycle frequency on mechanical behavior, Ma et al. (2013) studied the damage evolution under the frequencies of 0.025, 0.05 and 0.1 Hz and found that the damage and axial deformation decreases with the increasing of the frequencies. Fuenkajorn et al. (2010) explored the mechanical properties for two loading frequencies (0.001 and 0.03 Hz) and concluded that the effect of loading frequency on the salt strength appears to be small as compared to the impacts from the stress-related factors. Deng et al. (2017) conducted cyclic loading tests on sandstone at six different frequencies (1, 0.5, 0.2, 0.1, 0.05 and 0.02 Hz) and reported that a high frequency helps the energy dissipate and accelerates the damage. A study of loading speeds (Ren et al. 2013) showed that fatigue life changes very little as the loading speed changes; Momeni et al. (2015) found that fatigue life of monzogranite rock increases as an exponential function with increasing loading frequency, but energy density and hysteresis energy decrease as frequency increases. Attewell and Farmer (1973) carried out cyclic loading at the frequencies of 0.3, 2.5, 10 and 20 Hz and observed that high frequency increases the number of cycles to failure of dolomites. Similar conclusions were drawn by Liu et al. (2017) who reported that the tensile fatigue life increases, and the rock specimen is less fragmented with increasing frequency. Peng et al. (2020a, b) mentioned the different results of previous studies on frequency and ascribed them to the different experimental settings and the sensitivity factors of the equipment. They considered two test methods, namely the constant loading cycles and constant time. The results of the constant cycles

showed that the high frequency can harden the rock and improve its strength, but opposite results were observed for the constant time.

The published studies have explored the effects of the loading frequency; however, the effect is still debated. Several frequencies with small differences were tested in previous studies (Table 1). Moreover, the previous tests adopted the method of testing one sample only for one frequency, and no repeatability tests were performed. The results obtained by the test may be affected by the sample-to-sample variability, and contradictory conclusions are drawn. Additionally, in most published studies, the fatigue life is quantified by the cycle number. Thus, it is easy to conclude that a higher frequency induces a longer fatigue life because of the natural advantage of high frequency resulting in more cycles. At the same frequency, the cycle number can reflect the time from loading to failure and evaluating the service life. But when the frequencies are different, the cycle number must be multiplied by the cycle period, this being the loading time. Therefore, the larger number of cycles not always represent a longer service life.

Based on the above points, it is necessary to carry out a reliable and systematic experiment on the influence of frequency. The test method of changing the frequency by multi-step on one sample (stepped-frequencies cyclic loading tests) can eliminate the sample-to-sample variability and make full use of the small number of samples and is suitable to explore the effect of the frequency. In this paper, stepped-frequencies cyclic loading tests are carried out on rock salt. Based on the test results, the strain and dissipated energy under different frequencies are compared and analyzed. Further, the effects of frequency on the rock mechanical behavior are discussed.

## 2 Experimental Design and Test Scheme

### 2.1 Sample Preparation and Test Apparatus

The salt samples tested were from Pakistan. They have a relatively high purity of halite (more than 96%). They are transparent white or light red, and their average density is 2.14 g/cm<sup>3</sup>. Samples were processed into standard cylinders by wire cutting, with a size of  $\Phi 50 \times 100$  mm (Fig. 1a). The surfaces are dry-polished, and the parallelism of the ends is controlled within  $\pm 0.2$  mm. The average uniaxial compression strength obtained from three replicated tests is around 29 MPa with a variation of 0.84 MPa.

The cyclic tests were conducted on a digitally controlled electrohydraulic servo machine XTR01-01 (Fig. 1b). The testing machine includes a servo-controlled automatic triaxial pressurization and measurement system which can be used for conventional uniaxial or triaxial compression tests,

**Table 1** List of Papers and results of studies on the influence of cyclic loading frequency on rock

References	Material	Frequency, rate, period	Results
Ma et al. (2013)	Rock salt	0.025, 0.05, and 0.1 Hz	The axial strain rate and the proportion of the second stage to the entire deformation process decrease nonlinearly with increasing loading frequency
Fuenkajorn et al. (2010)	Rock salt	0.001 Hz, 0.03 Hz	The effect of loading frequency on the salt strength appears to be small as compared to the impacts from the maximum load and the loading amplitude
Deng et al. (2017)	Sandstone	1 Hz, 0.5 Hz, 0.2 Hz, 0.1 Hz, 0.05 Hz, 0.02 Hz	The higher the frequency, the larger the area of the hysteresis loop
Ren et al. (2013)	Rock salt	0.36 kN/s, 1 kN/s, 3 kN/s, 5 kN/s, 7 kN/s, 10 kN/s	Fatigue life changes very little as the loading speed changes; As the loading speed drops, the percentage of the transient and steady phase decreases while the percentage of the accelerating phase increases
Wang et al. (2021)	Rock salt	(cycle period) 1 h, 2 h, 4 h, 8 h	The shorter the period, the greater the cumulative irreversible deformation
Momeni et al. (2015)	Granite	0.1 Hz, 0.2 Hz, 1.5 Hz	Fatigue life increases as an exponential function with increasing loading frequency
Attewell and Farmer (1973)	Dolomite	0.3 Hz, 2.5 Hz, 10 Hz, 20 Hz	Frequency increase increases the number of cycles to failure
Liu et al. (2017)	Sandstone	0.1 Hz, 0.5 Hz, 1 Hz	As the loading frequency increases from 0.1, 0.5, to 1 Hz, the tensile fatigue life of specimens increases exponentially from 19, to 38 and then to 85 cycles
Zhao et al. (2014)	Limestone	0.5 Hz, 1.0 Hz, 1.5 Hz, 2.0 Hz, 2.5 Hz, 3.0 Hz	The average strain increment of each cycle reduces with the increase of loading frequency, and fatigue life increases with the increase of frequency
Zhu et al. (2017)	Gypsum	0.5 Hz, 1.0 Hz, 1.5 Hz, 2.0 Hz	A higher frequency induces a smaller plastic strain and fewer microstructures in each cycle, and prolongs fatigue life
Peng et al. (2020a, b)	Sandstone	0.1 Hz, 0.3 Hz, 0.5 Hz	The constant cycles method can harden the rock and improve its strength. But during the constant time method, the accumulation of irreversible deformation greatly increased and degraded the strength
He et al. (2018a, b)	Rock salt	0.5 Hz, 1 Hz, 2 Hz, 4 Hz	The higher the frequency, the fewer the cycles

creep tests, and cyclic load tests. In order to improve the data accuracy, the axial load sensor has been replaced with a capacity of 100 kN.

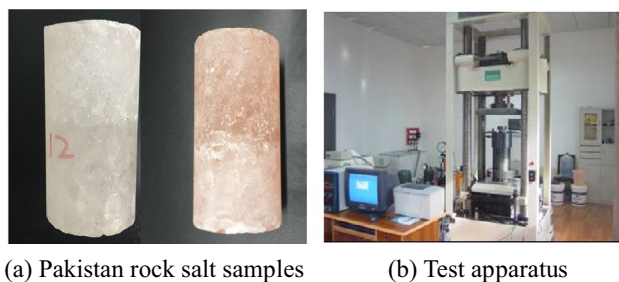
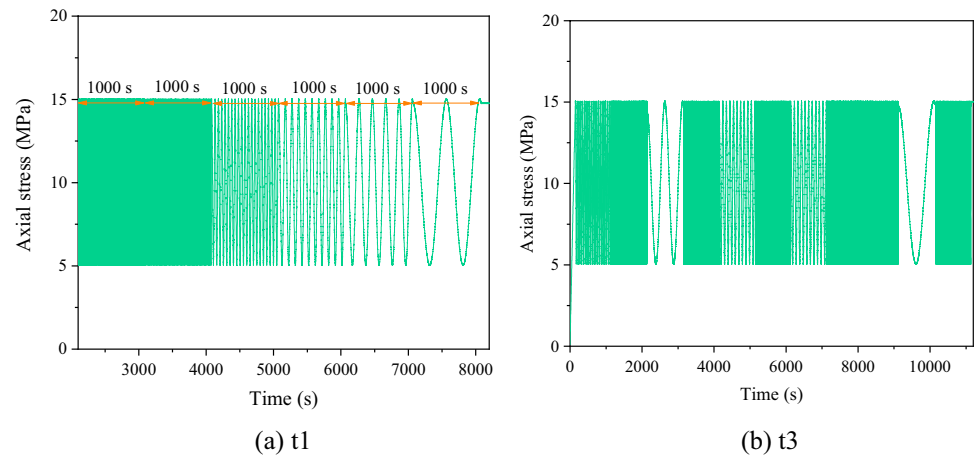


**Fig. 1** Test samples and test apparatus: (a) Pakistan rock salt samples, (b) Test apparatus

## 2.2 Testing Procedure

To identify the effects of loading frequencies on mechanical behavior, stepped cyclic loading tests with varying frequencies were conducted on five salt samples. Under each frequency, the time remained constant (1000 s) and the cycles varied. During a constant time of 1000 s, 1000 load cycles are implemented at a frequency of 1 Hz, and 10 load cycles at a frequency of 0.01 Hz, as shown in Fig. 2. The sine wave load was applied in the test with a cyclic stress range being 5 ~ 15 MPa. The maximum stress of 15 MPa is about 51.7% of the UCS, which can ensure that the samples will not undergo accelerated deformation during the test.

**Fig. 2** Loading history of samples t1 and t3: (a) t1 (b) t3



For the uniaxial cyclic tests, axial stress was first loaded at a constant rate of 0.1 MPa/s, followed by cyclic loading with stepped varying frequencies at the same cyclic stress. Three different frequencies change methods were applied, namely successively decreasing frequency, successively increasing frequency and arbitrarily changing frequency. To better analyze the test results, another two samples were tested under the conditions that the frequency was kept unchanged under a sine wave and a triangular wave with varying loading rate, respectively. The test scheme is shown in Table 2, where the samples t1–t5 correspond to different loading paths.

### 3 Test Results

#### 3.1 Overall Trend of the Axial Strain

Sample t4 was tested at a constant frequency of 0.001 Hz, and its axial stress–strain curve is shown in Fig. 3a. It can be observed that an obvious strain induced by the compaction

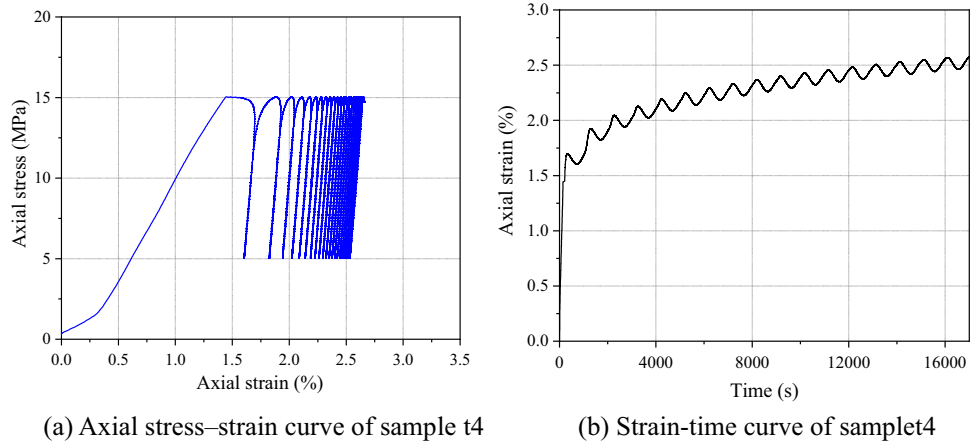
of the natural pores appears in the initial stage of static loading. After that, the sample enters the elastic deformation stage as the loading increases. When the sample is subjected to the cyclic loading, the strain caused by the first several cycles is significant, greater than that of the subsequent cycles. The evolution trend of the stress–strain curves changes from sparse to dense and the strain caused by one cycle gradually decreases, which reveals that the ability of the specimen to resist the irreversible deformation is successively enhanced by the cyclic loading. Figure 3b shows the evolution of strain with test time. The strain growth rate changes from fast to slow, and finally stabilizes. The curve undergoes transient and steady deformation stages, which is similar to the typical creep curve.

The stress–strain curve of sample t1 is displayed in Fig. 4a. Compared with the sample t4, the evolution of the stress–strain curves during this cyclic loading is slightly different. Sample t1 reaches the dense state quickly at the beginning of cyclic loading and the cycles remains dense when the frequencies change from 0.2 to 0.005 Hz. Only the sparse stress–strain curve appeared at the last frequency

**Table 2** The test scheme for salt samples

Sample no	Diameter (mm)	Height (mm)	Density (g/cm <sup>3</sup> )	Duration of each frequency (s)	Loading paths
t1	50.4	102.55	2.113	1000	Frequency decreases in the order: 1 Hz, 0.2 Hz, 0.1 Hz, 0.05 Hz, 0.02 Hz, 0.01 Hz, 0.005 Hz, 0.002 Hz
t2	49.96	102.52	2.155	1000	Frequency increases in the order: 0.002 Hz, 0.005 Hz, 0.01 Hz, 0.02 Hz, 0.05 Hz, 0.1 Hz, 0.2 Hz, 1 Hz
t3	49.93	102.23	2.148	1000	Frequency changes in the sequence: 0.02 Hz, 0.2 Hz, 0.002 Hz, 0.02 Hz, 0.01 Hz, 0.05 Hz, 0.01 Hz, 0.2 Hz, 0.1 Hz, 0.001 Hz, 0.05 Hz
t4	49.99	100.17	2.149	–	Cyclic loading range: 5–15 MPa; Frequency: 0.001 Hz
t5	50.07	99.77	2.134	2000	(Triangular wave) Loading rate: 1 MPa/s, 0.05 MPa/s, 0.01 MPa/s, 1 MPa/s

**Fig. 3** Test results of sample t4: (a) Axial stress–strain curve of sample t4, (b) Strain–time curve of sample t4



of 0.002 Hz. It can be seen from the strain–time curve in Fig. 4b that the strain jumped when the first frequency stage turned to the second stage. Then the strain increased gradually and smoothly as the frequency decreased, and the overall trend is similar to that of sample t4.

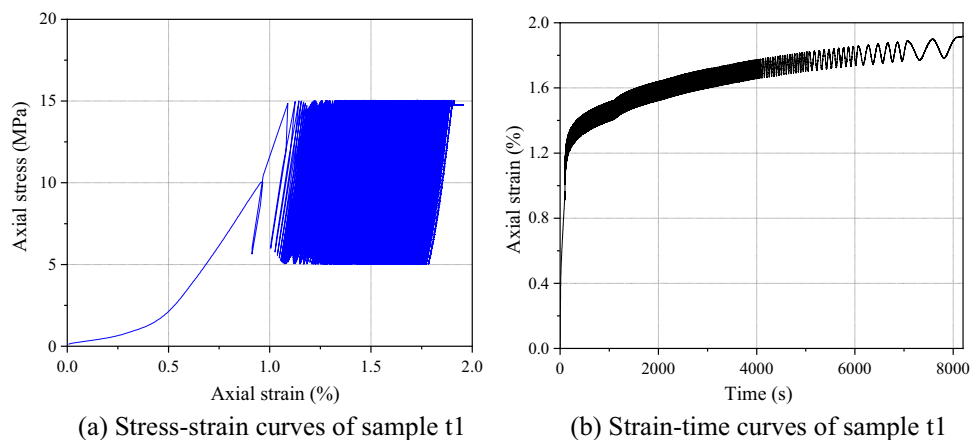
The strain jump only occurred at the frequency change from 1 to 0.2 Hz, and the reason may be that the data-collection interval (0.2 s) is too large to provide enough data for a high-frequency sine wave. When the frequency is 1 Hz, the stress is cycled between 5 and 15 MPa in 1 s, but the stress data collected may range from 6 to 14 MPa. As the frequency slows down, more data are collected to support the cyclic range (5–15 MPa). Therefore, the strain jump here is essentially caused by the missing data rather than the frequency. For a more accurate description of the cyclic loading, an interval of 0.1 s has been set.

In Fig. 5a, the stress–strain curves of sample t2 also changed from sparse to dense, but the sparse part is more obvious than that of samples t1 and t4, which means greater deformation has been produced by the first few cyclic loadings at slow frequency. As seen from the strain–time curve in Fig. 5b, the overall increase of axial strain is also consistent with that of sample t4. The sample first experienced

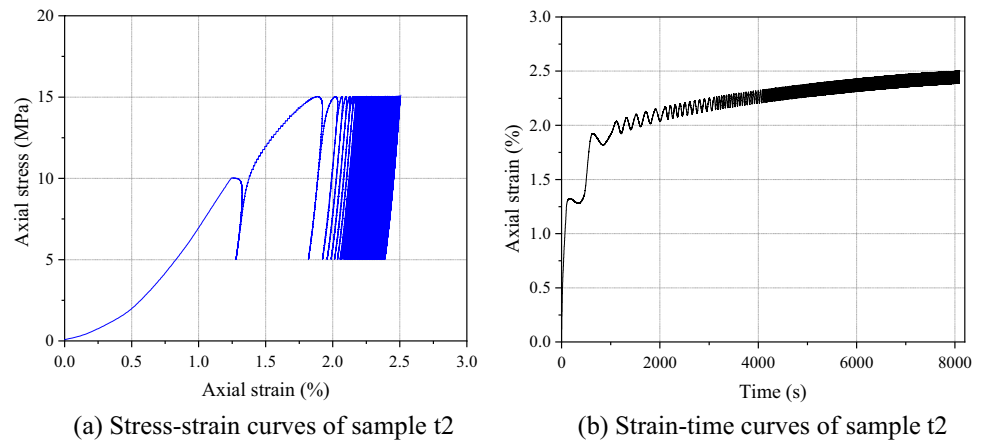
the transient deformation stage and then entered the steady deformation stage, during which no strain jump occurred.

Figure 6 shows the test results under the arbitrary frequency sequence. The cyclic curves evolve from sparse to dense in general (in Fig. 6a); however, as the frequency changes from high to low, the dense section turns to sparse. As observed from Fig. 6b, there is no strain jump on the strain curve, and the overall change is similar to that of sample t4. Comparing the strain–time curves of samples t1–t4 (as displayed in Fig. 7), the strain before the cyclic loading shows a noticeable difference. It reveals the influence of the sample-to-sample variability on test results. This is why the effect of the frequency is debated for the testing method using only one sample for each loading frequency. For the stepped-frequencies cyclic loading tests, the relative variation of the same sample at different frequencies is the key concern. The overall trend of the curves under changing frequency is consistent with that under constant frequency. The strain does not change significantly as the frequency increases or decreases, which is different from the results under the stepped changing stress (Han et al. 2020).

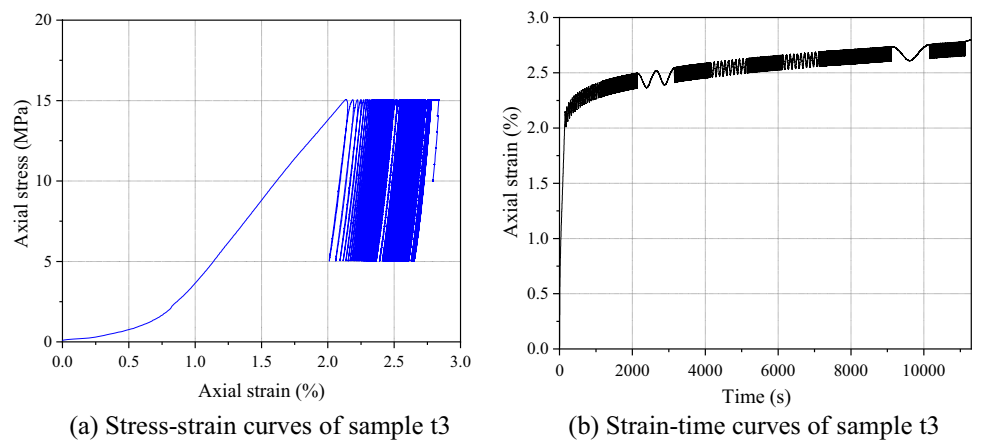
**Fig. 4** Test results of sample t1: (a) Axial stress–strain curve of sample t1, (b) Strain–time curve of sample t1



**Fig. 5** Test results of sample t2: (a) Axial stress–strain curve of sample t2, (b) Strain–time curve of sample t2



**Fig. 6** Test results of sample t3: (a) Axial stress–strain curve of sample t3, (b) Strain–time curve of sample t3



### 3.2 The Strain Induced by a Frequency Stage

To inspect the effect of the frequency on deformation, the induced strain during a frequency stage (named stage

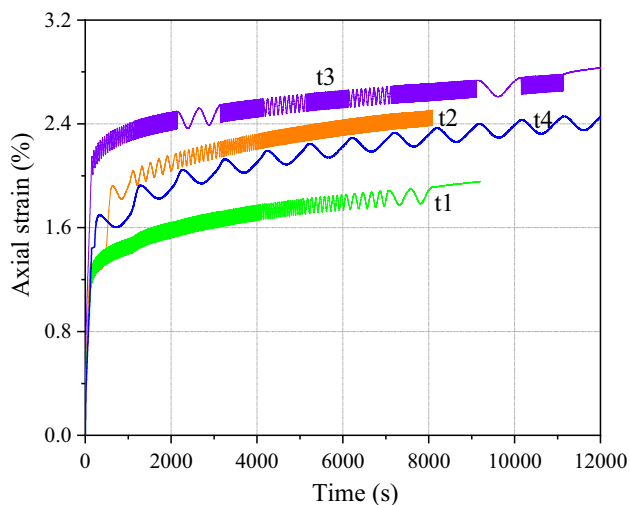


**Fig. 7** The strain–time curves of samples t1–t4

strain) was obtained and analyzed in detail. As observed from Fig. 8, the stage strain of sample t4 decreases gradually with the increasing of the stages. The downward trend becomes slower, indicating that the ability of the sample to resist deformation had been improved with the crystal compaction. Generally, the evolution of samples t1–t3 follow the same trend and the strain decreases gradually with the increasing of the stages. In the magnified image, the strain fluctuation only appears in sample t3. This may be because the frequency affects the deformation slightly. When the frequency decreases or increases orderly, the strain just follows the inherent trends and is not affected by the small (only two times) change of adjacent frequencies. When the frequencies change arbitrarily, the change range between adjacent frequencies can reach 100 times. In this way, the deformation fluctuations induced by the change of frequencies are reflected in the inherent deformation trend. The green dotted line in Fig. 8 shows that the strain in the 3<sup>rd</sup> and 10<sup>th</sup> stages (corresponding to the frequency of 0.002 Hz and 0.001 Hz), is much smaller than the adjacent frequencies. It indicates that the smaller strain of the 3<sup>rd</sup> and 10<sup>th</sup> stage is mostly caused by the slow frequency, and the stage strain increases as the frequency increases.

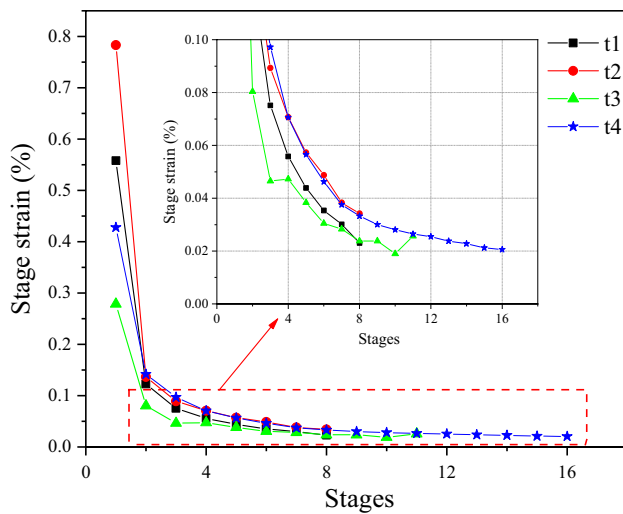


Fig. 8 The stage strain evolution of samples t1-t4

To further verify this conclusion, the stage strain of sample t5 under a triangular wave is analyzed. In Fig. 9a, the stress–strain curve is already in a dense state at the beginning of cyclic loading owing to the previous stress maintenance. Hereafter, the curves become sparse as the loading rate decreases. It can be seen from the strain history curve (Fig. 9b) that the overall trend of the strain–time curve is similar to that of the curve under a sine wave and grows smoothly without strain jump.

The stage strain for each loading rate of sample t5 is calculated. The stage strain of 1 MPa/s is 0.0502%, the stage strain of 0.05 MPa/s is 0.0199%, and the stage strain of 0.01 MPa/s is 0.0149%. The strain decreases gradually, conforming to the inherent deformation trend under cyclic loading. At the latter stage of 1 MPa/s, the increased strain from 8368 to 9120 s has reached the stage strain under the loading rate of 0.01 MPa/s, which was produced in 2000s. It can be inferred that a faster loading rate produces a larger stage strain, which is consistent with the result of sample t3.

Fig. 9 Test results of sample t5: (a) Axial stress–strain curve of sample t5, (b) Strain–time curve of sample t5

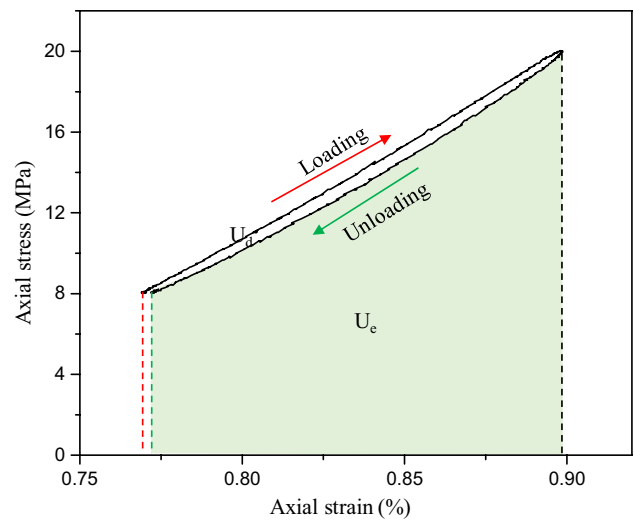
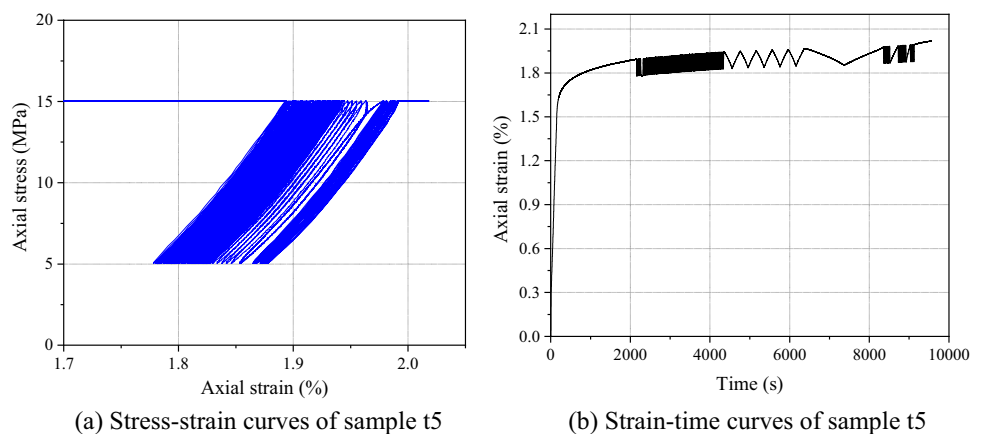


Fig. 10 The energy composition of the cyclic strain–stress curve

### 3.3 Dissipated Energy

Figure 10 shows a complete loading–unloading curve, where the area enclosed by the loading and unloading curves represents the dissipated energy, which is dissipated through the internal friction of the material or local damage (such as cracking, plastic hinge rotation (Zhu et al. 2017) (Deng et al. 2017)). The dissipated energy is an important index for evaluating the internal damage of the sample, and a large dissipated energy represents a large damage. The energy dissipated in one cycle is as follows:

$$\Delta U_{di} = \int_{\epsilon_{i1+}}^{\epsilon_{i2+}} \sigma_1 d\epsilon_1 - \int_{\epsilon_{i2-}}^{\epsilon_{i1-}} \sigma_1 d\epsilon_1 \quad (1)$$

The accumulated dissipated energy of a frequency stage (stage dissipation energy) is as follows:

$$\Delta U_d = \sum_1^i \Delta U_{di} \quad (2)$$

Figure 11 displays the loading and unloading curves of sample t5 at different loading rates. The loading and unloading curve forms a closed loop like a willow leaf when the rate is 1 MPa/s. However, as the loading rate decreases, the cyclic curve is not closed, forming a large unclosed curve. In Fig. 11, the loading rates of the triangular wave are 1 MPa/s, 0.05 MPa/s, 0.01 MPa/s and 1 MPa/s, and the corresponding individual dissipation energy is 0.388 kJ/m<sup>3</sup>, 0.960 kJ/m<sup>3</sup>, 2.033 kJ/m<sup>3</sup>, and 0.340 kJ/m<sup>3</sup>, respectively. The individual dissipation energy increases nonlinearly and discernibly as the loading rate decreases. The stage dissipated energy calculated through Eq. (2) is represented in Fig. 12. The stage dissipation energy from left to right is 14.033 kJ/m<sup>3</sup>, 4.519 kJ/m<sup>3</sup>, 3.540 kJ/m<sup>3</sup>, and 9.321 kJ/m<sup>3</sup>. The stage dissipated energy decreases with decreasing loading rate, which is contrary to the results of individual dissipated energy. This can be explained by the fact that the growth rate of the individual dissipated energy is much smaller than the decrease rate of the loading rate itself. For example, 1 MPa/s is 20 times 0.05 MPa/s, but the individual dissipation energy at 0.05 MPa/s is only 2.5 times that at 1 MPa/s. During a constant loading time, the stage dissipated energy can be calculated by multiplying the individual dissipated energy with the number of cycles, which is linearly positively related to the loading rate. Considering the significance of the loading rate, the stage dissipation energy is mainly controlled by the loading rate and not by the individual dissipation energy. That is, a quicker loading rate results in more cycles and generates more dissipated energy in a constant time.

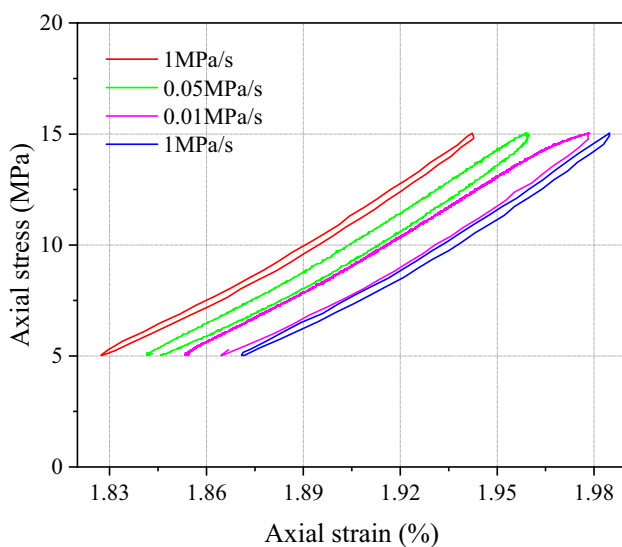


Fig. 11 The loading and unloading curves of sample t5

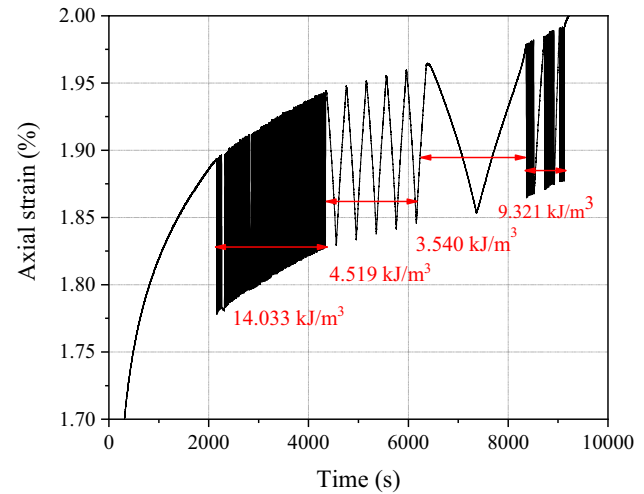


Fig. 12 Stage dissipated energy of sample t5 at different loading rates

Based on the analysis of sample t5, the evolution of stage dissipated energy of samples t1–t4 is statistically compared. As shown in Fig. 13, the stage dissipated energy of sample t4 decreases with the stages. Its overall trend is similar to that of the stage strain in Fig. 8. In the first two stages, the dissipated energy decreases significantly, and then the dissipated energy gradually decreases and tends to stabilize.

The curves in Fig. 14 show the stage dissipated energy evolution with the stages under different frequency change sequences. The decreasing trend of the stage dissipated energy of sample t1 is similar to that of sample t4, but the dissipation energy of sample t1 decreases more obviously due to the decrease of the frequency in the subsequent stages. The dissipated energy of sample t2 shows a U-shaped

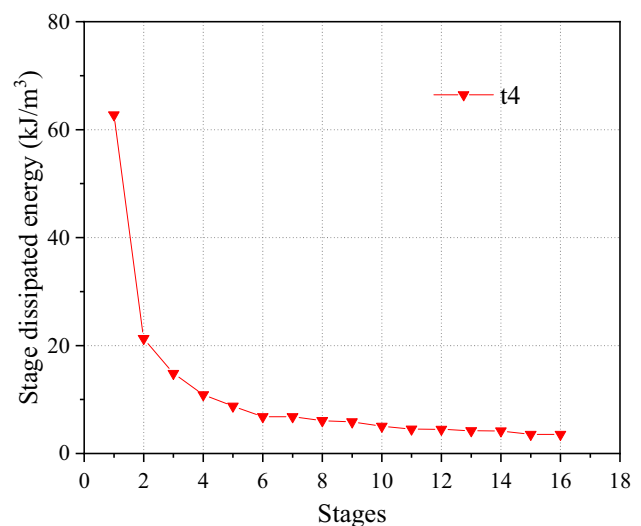
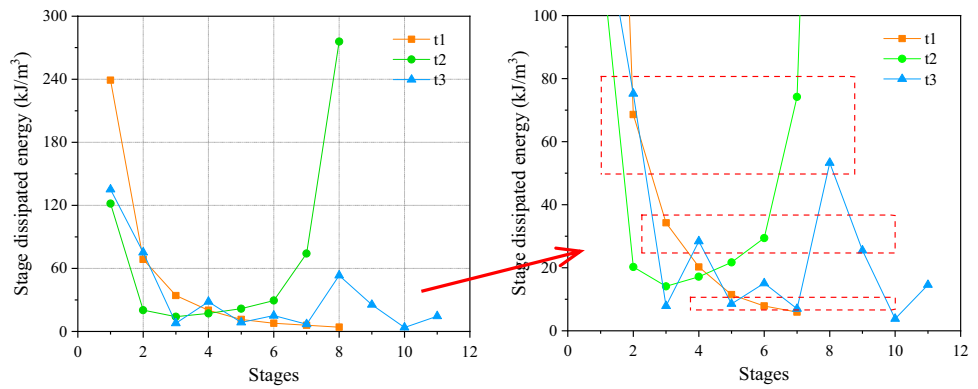


Fig. 13 Stage dissipated energy sample t4



**Fig. 14** Stage dissipated energy for three different changing frequency sequences



change when the frequencies increase with stages. In the first few stages, the evolution is consistent with the inherent decrease properties. Starting from the fourth stage, the dissipated energy increases due to the increase in frequency, and the curve turns into an upward trend. The stage dissipation energy of the sample t3 whose frequency changes irregularly, generally decreases with the loading stages, but fluctuates with the frequency change during the later stages. This is mainly reflected in the significant increase of dissipated energy as the frequency increases sharply.

In general, the faster the frequency, the greater the stage energy dissipation. Seen from the enlarged picture in Fig. 14, the dissipated energy framed by the dashed box is generated by different samples at different stages but under the same frequency. The numerical values of the stage dissipated energy are very close to each other. Based on the stage dissipation energy in the dashed box, the average stage dissipation energy under one frequency is obtained. Figure 15 shows the fitting relationship between stage dissipated energy and frequency. The stage dissipated energy increases nearly as a power function with the frequency.

Since the relationship between stage dissipated energy and frequency is explored, the evolution of the individual dissipated energy under different frequencies can be inferred. Assuming the dissipated energy of each cycle is uniform, the individual dissipated energy under different frequencies can be calculated by dividing the stage dissipated energy (in Fig. 15) by the number of cycles. The result is displayed in Fig. 16, where the individual dissipated energy decreases with increasing frequency, also in a power function relationship. According to the fitting equations, the individual dissipated energy ( $U_{id}$ ) and stage dissipated energy ( $U_{sd}$ ) can be expressed as follows:

$$U_{id} = a_i f^{b_i} \tag{3}$$

$$U_{sd} = a_s f^{b_s} \tag{4}$$

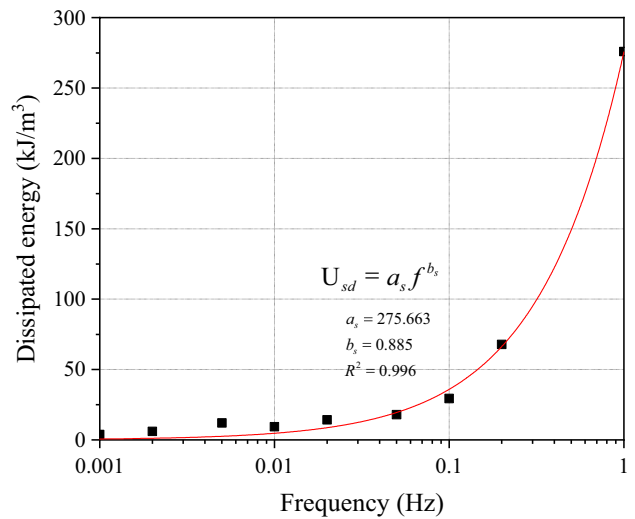


**Fig. 15** The relationship between frequency and stage dissipated energy

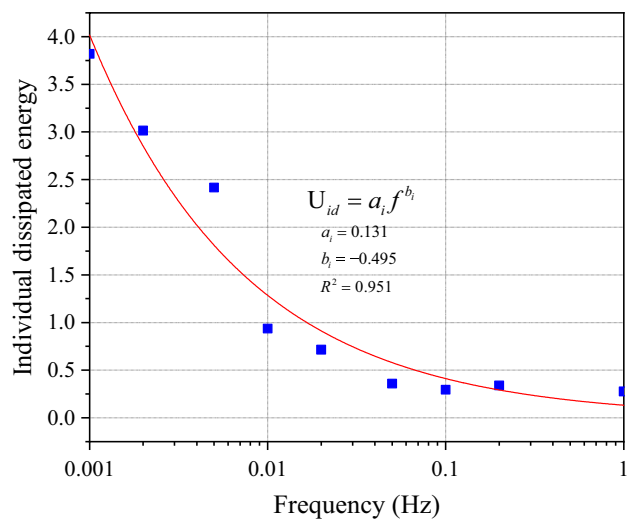


**Fig. 16** The relationship between frequency and individual dissipated energy

where the function coefficients  $a_i$ ,  $a_s$ ,  $b_i$  and  $b_s$  are fitted as 0.131, 275.663,  $-0.495$  and  $0.885$ , respectively;  $f$  is the frequency.

There is a connection between  $U_{id}$  and  $U_{sd}$ , established as follows:

$$U_{sd} = U_{id} \cdot (f \Delta t) \quad (5)$$

where  $\Delta t$  is the stage time (1000 s).

Obtained from the Eq. (3)–(5), the coefficients  $a_s$  and  $b_s$  can be expressed as follows

$$\begin{aligned} a_s &= a_i \Delta t \\ b_s &= b_i + 1 \end{aligned} \quad (6)$$

To meet the monotonic decrease rule of the individual dissipated energy and the monotonic increase rule of the stage dissipation energy, their first derivatives concerning frequency must satisfy the following relationship:

$$\begin{aligned} a_i b_i f^{b_i-1} &< 0 \\ a_s b_s f^{b_s-1} &> 0 \end{aligned} \quad (7)$$

Since  $f$ ,  $a_i$  and  $a_s$  are greater than 0, the coefficients  $b_i$  and  $b_s$  should be as follows:

$$\begin{aligned} b_i &< 0 \\ b_s &= b_i + 1 > 0 \end{aligned} \quad (8)$$

Thus, the range of the coefficient  $b_i$  must be between  $-1$  and  $0$ .

Although the fitting values of the function coefficients do not exactly follow the relationship of Eq. (6), the fitting value of  $b_i$  is between  $-1$  and  $0$ , which agrees with the theoretical result. These fitting values are reasonable with acceptable errors. It illustrates that the power function could reliably describe the influence of frequency.

## 4 Discussion

In this paper, the influence of frequency on deformation and dissipated energy is studied. However, the fatigue life cannot be obtained directly since the samples did not fail. Extensive research has investigated fatigue life. For example, Ge et al. (2003) proposed that fatigue life is controlled by the axial strain, which has also been unanimously recognized in much related research. He et al. (2018a, b; 2018a, b) mentioned that the total dissipation energy of damage under different frequencies remains unchanged, and the fatigue life is determined by the dissipation energy in the steady-strain stage. Relying on the view of constant total dissipation energy, the fatigue life under different frequencies can be inferred.

Fatigue life is always quantified by the number of cycles. But sometimes the service life is worthy of attention rather

than the number of cycles in many geotechnical projects. These two quantification methods can be derived from the equation of individual dissipated energy (Eq. (3)), shown as

$$N = \frac{U_k}{U_{id}} = \frac{U_k}{a_i f^{b_i}} \quad (9)$$

$$t = N \cdot T = \frac{U_k}{a_i f^{b_i}} \cdot \frac{1}{f} \quad (10)$$

where  $U_k$  is the constant total dissipation energy;  $N$  is the total number of cycles;  $T$  is the cycle period;  $t$  is the total time.

From Eq. (8), it can be seen that the total number of cycles increases with increasing frequency, but the result of the total time is the opposite. In other words, if the rock salt fails under a higher frequency, it will experience more cycles, but a shorter loading time. To some extent, this power–function relationship explains the contradictory results which are found through two loading methods in research (Peng et al. 2020a, b).

The test results show that the stage strain and stage dissipated energy increase with the increase of cycle frequency. From the energy storage perspective, when the salt cavern is used for storing compressed air with the same operating pressure for a period of time, the surrounding rock shrinks more severely and the damage of the surrounding rock is also more serious than that used for storing natural gas. On the other hand, to achieve the same service life as storing natural gas, the operating pressure of compressed gas storage should be more conservative to reduce the damage and deformation caused by high-frequency loads.

## 5 Conclusions

Based on the uniaxial stepped cyclic loading of salt samples, the following main points are inferred:

Deformation of rock salt is slightly affected by the changing frequency, and the overall trends of the strain history under three changing methods are similar to that of the creep test. The impact on deformation is small but still exists. Only under the arbitrarily changing method (when the adjacent frequencies differ greatly) can it be detected that a higher frequency prompts larger stage deformation.

Dissipated energy is obviously affected by the frequency change. The individual dissipated energy decreases with the increase of frequency, while the stage dissipated energy shows the opposite. The change of the individual dissipated energy and the stage dissipated energy with frequency can be well fitted by a power function. Moreover, the exponent coefficient ( $b_i$ ) of the power function for the individual dissipated energy is between  $-1$  and  $0$ .

Based on the test results, it can be inferred that the damage and deformation of the rock surrounding a salt cavern are relatively large when the cyclic loading is fast. The relevant safety rules should be more stringent under higher frequency conditions. This means that when the salt cavern is used for compressed air energy storage, the operating parameters should be more conservative compared with those when storing natural gas.

**Acknowledgements** The work presented in this paper is supported by the National Natural Science Foundation of China (Grant No. 5187041724). The authors wish to offer their gratitude and regards to prof. Jaak J Daemen, Mackay School of Earth Sciences and Engineering, University of Nevada, for his thoughtful proofreading of this paper.

## Declarations

**Conflict of Interest** The authors declare that no conflict of commercial or associative interest exists in the submission of this manuscript,

## References

- Attewell PB, Farmer IW (1973) Fatigue behavior of rock. *Int J Rock Mech Min Sci Geomech Abs* 10:1–9
- Chen J, Du C, Jiang D, Fan J, He Y (2016) The mechanical properties of rock salt under cyclic loading-unloading experiments. *Geomech Eng* 10:325–334
- Chen C, Xu T, Heap MJ, Baud P (2018) Influence of unloading and loading stress cycles on the creep behavior of Darley Dale Sandstone. *Int J Rock Mech Min Sci* 112:55–63
- Deng H, Hu Y, Li J, Wang Z, Zhang X, Zhang H (2017) Effects of frequency and amplitude of cyclic loading on the dynamic characteristics of sandstone. *Rock Soil Mech* 38:3402–3411
- Fan J, Liu W, Jiang D, Chen J, Tiedeu WN, Daemen JJK (2020) Time interval effect in triaxial discontinuous cyclic compression tests and simulations for the residual stress in rock salt. *Rock Mech Rock Eng* 53:4061–4076
- Fuenkajorn K, Phueakphum D (2010) Effects of cyclic loading on mechanical properties of Maha Sarakham salt. *Eng Geol* 112:43–52
- Ge X, Jiang Y, Lu Y, Ren J (2003) Testing study on fatigue deformation law of rock under cyclic loading. *Chin J Rock Mech Eng* 22:1581–1585
- Guo Y, Yang C, Wang L, Xu F (2018) Effects of cyclic loading on the mechanical properties of mature bedding shale. *Adv Civ Eng* 2018:1–9
- Han Y, Ma H, Yang C, Zhang N, Daemen J (2020) A modified creep model for cyclic characterization of rock salt considering the effects of the mean stress, half-amplitude and cycle period. *Rock Mech Rock Eng* 53:3223–3236
- He MM, Huang BQ, Zhu CH, Chen YS, Li N (2018a) Energy dissipation-based method for fatigue life prediction of rock salt. *Rock Mech Rock Eng* 51:1447–1455
- He MM, Li N, Huang BQ, Zhu CH, Chen YS (2018b) Plastic strain energy model for rock salt under fatigue loading. *Acta Mech Solida Sin* 31:322–331
- Hu B, Yang S-Q, Xu P, Cheng J-L (2019) Cyclic loading–unloading creep behavior of composite layered specimens. *Acta Geophys* 67:449–464
- Jiang D, Fan J, Chen J, Li L, Cui Y (2016) A mechanism of fatigue in salt under discontinuous cycle loading. *Int J Rock Mech Min Sci* 86:255–260
- Khaledi K, Mahmoudi E, Datcheva M, Schanz T (2016) Stability and serviceability of underground energy storage caverns in rock salt subjected to mechanical cyclic loading. *Int J Rock Mech Min Sci* 86:115–131
- Liu Y, Dai F, Xu N, Zhao T (2017) Cyclic flattened Brazilian disc tests for measuring the tensile fatigue properties of brittle rocks. *Rev Sci Instrum* 88:083902
- Liu Y, Dai F, Feng P, Xu N-w (2018) Mechanical behavior of intermittent jointed rocks under random cyclic compression with different loading parameters. *Soil Dyn Earthq Eng* 113:12–24
- Ma L, Liu X, Wang M, Xu H, Hua R, Fan P, Jiang S, Wang G, Yi Q (2013) Experimental investigation of the mechanical properties of rock salt under triaxial cyclic loading. *Int J Rock Mech Min Sci* 62:34–41
- Ma L, Wang M, Zhang N, Fan P, Li J (2017) A variable-parameter creep damage model incorporating the effects of loading frequency for rock salt and its application in a bedded storage cavern. *Rock Mech Rock Eng* 50:2495–2509
- Momeni A, Karakus M, Khanlari GR, Heidari M (2015) Effects of cyclic loading on the mechanical properties of a granite. *Int J Rock Mech Min Sci* 77:89–96
- Peng K, Zhou J, Zou Q, Zhang J, Wu F (2019) Effects of stress lower limit during cyclic loading and unloading on deformation characteristics of sandstones. *Constr Build Mater* 217:202–215
- Peng H, Fan J, Zhang X, Chen J, Li Z, Jiang D, Liu C (2020a) Computed tomography analysis on cyclic fatigue and damage properties of rock salt under gas pressure. *Int J Fatigue* 134:105523
- Peng K, Zhou J, Zou Q, Song X (2020b) Effect of loading frequency on the deformation behaviours of sandstones subjected to cyclic loads and its underlying mechanism. *Int J Fatigue* 131:105349
- Ren S, Bai Y, Zhang J, Jiang D, Yang C (2013) Experimental investigation of the fatigue properties of salt rock. *Int J Rock Mech Min Sci* 64:68–72
- Wang T, Yang C, Chen J, Daemen JJK (2018) Geomechanical investigation of roof failure of China's first gas storage salt cavern. *Eng Geol* 243:59–69
- Wang J, Zhang Q, Song Z, Zhang Y (2021) Experimental study on creep properties of salt rock under long-period cyclic loading. *Int J Fatigue* 143:106009
- Yin H, Yang C, Ma H, Shi X, Chen X, Zhang N, Ge X, Liu W (2018) Study on Damage and repair mechanical characteristics of rock salt under uniaxial compression. *Rock Mech Rock Eng* 52:659–671

**Publisher's Note** Springer Nature remains neutral with regard to jurisdictional claims in published maps and institutional affiliations.

Springer Nature or its licensor holds exclusive rights to this article under a publishing agreement with the author(s) or other rightsholder(s); author self-archiving of the accepted manuscript version of this article is solely governed by the terms of such publishing agreement and applicable law.